ACS Catalysis

Research Article

pubs.acs.org/acscatalysis

Effects of the Support on the Performance and Promotion of (Ni)MoS_2 Catalysts for Simultaneous Hydrodenitrogenation and Hydrodesulfurization

Oliver Y. Gutiérrez,* Srujan Singh, Eva Schachtl, Jeongnam Kim, Elena Kondratieva, Jennifer Hein, and Johannes A. Lercher*

Department of Chemistry and Catalysis Research Center, TU München, Lichtenbergstrasse 4, D-84747 Garching, Germany

Supporting Information

ABSTRACT: MoS_2 and Ni-promoted MoS_2 catalysts supported on γ-Al_2O_3, siliceous SBA-15, and Zr- and Ti-modified SBA-15 were explored for the simultaneous hydrodesulfurization (HDS) of dibenzothiophene (DBT) and hydrodenitrogenation (HDN) of *o*-propylaniline (OPA). In all cases, OPA reacted preferentially via initial hydrogenation, and DBT was converted through direct sulfur removal. HDN and HDS activities of MoS_2 catalysts are determined by the dispersion of the sulfide phase. Ni promotion increased its dispersion and activity for DBT HDS and also increased the rate of HDN via enhancing the rate of hydrogenation. On nonpromoted MoS_2 catalysts, HDS was strongly inhibited by NH_3, and the addition of Ni dramatically reduced this inhibiting effect. The conclusion is that HDS is proportional to the concentration of Mo and Ni on the edges of sulfide particles. In contrast, the direct hydrodenitrogenation of OPA occurs only on accessible Mo cations and, hence, decreases with increasing Ni substitution. The nature of the support influences the dispersion of the nonpromoted catalysts as well as the decoration degree of Ni on the edges of the Ni−Mo−S phase. Furthermore, the acidity of the support influences the acidity of the supported sulfide phase, which may play an important role in HDN.

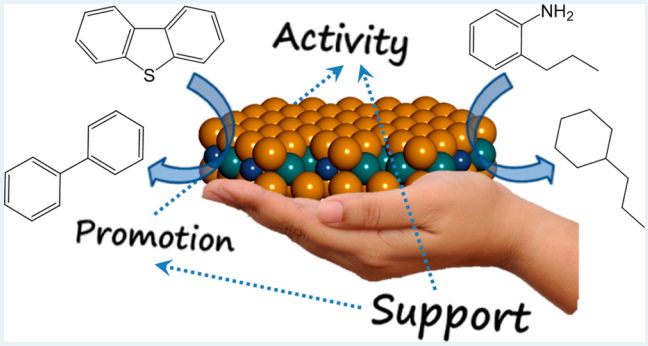

KEYWORDS: *HDS, HDN, SBA-15, MoS_2, Ni promotion, support effect*

INTRODUCTION

In recent decades, the concern for minimizing the environmental impact of pollutants resulting from the use of transportation fuels has driven a large body of research focused on removing heteroatoms from hydrocarbon energy carriers.[1−3] Thus, designing hydrotreating catalysts with improved activity compared to Co(Ni)-promoted MoS_2 supported on Al_2O_3 has been an important research theme. A promising strategy to achieve this has been related to alternative supports because the properties of the sulfide phase have been observed to be strongly affected by the nature of the catalyst support.[4] Diverse well-defined materials, including mixed oxides, zeolites, and mesoporous molecular sieves have been tested as hydrotreating supports.[4−9] Among the latter, SBA-15 has attracted attention because of its outstanding hydrothermal stability and textural properties.[10−13] Several strategies have been followed to prepare MoS_2 catalysts supported on SBA-15 with high activity comparable with industrial catalysts.[12,14,15] The modification of SBA-15 by heteroatom incorporation has been found to yield MoS_2-based catalysts with similar or higher hydrodesulfurization (HDS) and hydrodenitrogenation (HDN) activity than Al_2O_3-supported counterparts.[14−19] In turn, those catalytic systems have been widely tested in HDS of model compounds to elucidate the origin of the positive effect of the support.[20−23] However, there are only few reports addressing the effect of those materials on the HDN activity of the supported MoS_2 phase via exploring the reactivity toward HDN of model reactants.[24,25] Furthermore, the application of modified mesoporous materials as supports opens the possibility of finely tuning the interaction with the active phase (and therefore, its properties), allowing establishing unambiguous structure−activity correlations.

In this work, we present the results of the simultaneous HDN and HDS of *o*-propylaniline (OPA) and dibenzothiophene (DBT) on MoS_2 and Ni-MoS_2 catalysts supported on siliceous as well as Ti- or Zr-modified SBA-15-type materials and Al_2O_3. The physicochemical properties of the sulfide catalysts were explored by elemental analysis, transmission electron microscopy, physisorption of N_2, NO chemisorption, and adsorption of CO followed by IR spectroscopy. The results indicate that the dispersion, the morphology, and the effectiveness of the Ni promotion of the MoS_2 phase—all

Received: January 10, 2014
Revised: March 27, 2014
Published: April 11, 2014

   dx.doi.org/10.1021/cs500034d | ACS Catal. 2014, 4, 1487−1499

affecting the HDN and HDS to varying extent—strongly depend on the nature of the support. The nature of the active sites for HDN and HDS is discussed on the basis of kinetic analysis and probing of the active phase.

EXPERIMENTAL SECTION

Synthesis of Supports. Pure siliceous SBA-15 was synthesized according to the following procedure: The required amount of surfactant (P123, Aldrich) was added to a 0.3 M HCl aqueous solution, keeping a solution/surfactant wt % ratio of 19. The mixture was stirred at 308 K until a homogeneous solution was obtained, and then TEOS (tetraethyl orthosilicate, ≥99%, Aldrich) was added at a TEOS/surfactant wt % ratio of 1.6. The mixture was kept at 308 K for 24 h and after that at 353 K for 24 h more. At the end of the hydrothermal procedure, the formed solid was filtered, dried at 333 K, and washed with excess ethanol (≥99.5%, Aldrich). The product was treated in flowing air at 773 K for 4 h, increasing the temperature by 2.5 K·min^{-1}. The Ti- and Zr-modified SBA-15 samples were prepared by incipient wetness impregnation. The first step was the preparation of solutions of zirconium(IV) propoxide (70 wt % in 1-propanol, Aldrich) and titanium(IV) isopropoxide (≥97.0%, Aldrich) in high-purity ethanol (anhydrous, Sigma-Aldrich). Samples of SBA-15 were impregnated with the solutions. After drying, the solids were calcined in flowing air at 823 K for 5 h, initially increasing the temperature by 10 K·min^{-1}. The alumina used here was a sample from Chevron with BET surface area of 237 m^2·g^{-1}. In the following, SBA-15 denotes the pure siliceous material, whereas Zr-SBA and Ti-SBA denote the Zr- and Ti-modified materials, respectively.

Synthesis of Catalysts. Mo-containing oxide precursors were prepared by impregnation of the supports with aqueous solutions of ammonium molybdate tetrahydrate (99.98%, Aldrich). The Ni-added materials were obtained by subsequent impregnations of the Mo oxide precursors with aqueous solutions of Ni (II) nitrate hexahydrate (≥98.5%, Aldrich). The pH of the precursor solutions was around 6. The materials were calcined at 823 K for 5 h, initially increasing the temperature by 10 K·min^{-1} in flowing air after each impregnation. Prior to the physicochemical characterization and the catalytic testing, the sulfide catalysts were obtained by thermal treatment of the oxide precursors at 673 K in a flow of H_2S (10 vol %) in H_2 for 6 h. All characterization results reported here correspond to the sulfide catalysts. In the following, the nonpromoted catalysts are denoted as MoS_2/support, whereas the Ni-promoted catalysts are referred to as Ni-MoS_2/support.

Chemical and Physicochemical Characterization. The elemental compositions of the sulfide catalysts were determined by atomic absorption spectroscopy using a UNICAM 939 spectrometer. The textural properties of the materials were derived from N_2-physisorption measurements performed in a PMI automated sorptometer at liquid N_2 temperature. Prior to N_2-physisorption experiments, the materials were outgassed at 523 K for 6 h. Specific surface areas were calculated by the BET method, and pore size distributions were determined from the desorption isotherms by the BJH method. X-ray diffractograms of the catalysts were obtained in a Philips X'Pert Pro System instrument (Cu Kα1 radiation, 0.154 056 nm) operating at 45 kV and 40 mA using a step size of 0.017° (2θ) and 115 s as the count time per step. To perform transmission electron microscopy (TEM) analyses, samples of the catalysts were ground, suspended in ethanol, and ultrasonically dispersed. Dispersion drops were applied on a copper−carbon grid, and the measurements were carried out in a JEOL JEM-2011 electron microscope with an accelerating voltage of 120 keV. Statistical analysis of the length and stacking degree of the MoS_2 phase was done by using the ImageJ software to treat digital images acquired in the TEM measurements. The counting included at least 200 crystallites distributed on 10 micrographs (taken in different places of the grid) or more per sample.

CO adsorption followed by IR spectroscopy was performed using self-supported wafers (5−10 mg·cm^{-2}) of the oxide material that were placed into a dedicated IR cell. The sample was treated in situ at 673 K for 2 h under a flow of H_2S (10 vol %) in H_2 and then flushed with He for 1 h at 673 K. After cooling to room temperature, the cell was evacuated to a residual pressure of 5×10^{-6} mbar. CO was admitted to the cell at 123 K up to an equilibrium pressure of 1 mbar CO, and the spectra were recorded. A Nicolet 6700 FT-IR spectrometer equipped with a MCT detector with a resolution of 4 cm^{-1} was used. The background was subtracted in all reported spectra, which were normalized to a disc of 1 cm^{-2} and 10 mg.

The IR spectra were deconvoluted by superimposition of Lorentzian−Gaussian curves using the OMNIC software following recommendations of specialized literature.[26,27] The number of bands was fixed to four and five for MoS_2 and Ni-MoS_2 materials, respectively, according to the band positions and assignments described in the Results section. The deconvolution was started with curves fixed in wavenumbers and full widths at half maxima; however, it was noticed during the fitting procedure that the position of the bands strongly depended on the support. Thus, the fitting optimization was performed allowing the band positions to vary. This procedure has been proven insightful for the analysis of IR spectra of CO adsorbed on sulfide catalysts.[28]

NO adsorption experiments were performed at room temperature after in situ treatment of the samples at 673 K for 2 h under a flow of H_2S (10 vol %) in H_2. While the sample was kept in He, pulses of 10 vol % NO in He were injected periodically until adsorption was not observed. The adsorption of NO was monitored using a Balzers mass spectrometer, and the total concentration of NO adsorbed was calculated as the sum of NO uptakes per pulse.

Simultaneous HDS and HDN Activity Tests. The activity of the catalysts was evaluated in the simultaneous HDN of OPA and HDS of DBT in a batch mode. A sample of each sulfide catalyst (0.25 g) was transferred to the autoclave (Parr Instruments, 300 mL) under inert atmosphere, and the reactions were carried out at 573 K and 7.3 MPa of H_2 pressure using a reactant solution of DBT (0.0238 M) and OPA (0.0273 M) in tetradecane. The reactor was filled with 60 mL of solution per reaction. Aliquots were taken periodically and analyzed off-line by gas chromatography with a HP 6890 GC equipped with a flame ionization detector and an Agilent DB-17 capillary column. Reaction rate constants (k_i) were calculated following Langmuir−Hinshelwood formalisms as described in the Results section. Turnover frequencies were calculated by simply dividing k_i by the product of the initial molar concentration of the reactant (DBT or OPA) and a relevant magnitude (i.e., the concentration of adsorbed NO, integrated areas of the CO-IR adsorption bands, and fraction of Mo atoms at the edges of MoS_2 slabs).

dx.doi.org/10.1021/cs500034d | ACS Catal. 2014, 4, 1487−1499

RESULTS

Characterization. Table 1 compiles the elemental composition of MoS_2 and Ni-MoS_2 catalysts (the elemental

Table 1. Elemental Content (mol %) of the MoS_2 and Ni-MoS_2 Catalysts

	MoS_2 catalysts				Ni-MoS_2 catalysts			
support →	Al_2O_3	SBA-15	Ti-SBA	Zr-SBA	Al_2O_3	SBA-15	Ti-SBA	Zr-SBA
S	3.87	3.47	3.36	3.44	2.90	2.82	2.72	2.99
Ti			2.55				1.75	
Zr				1.58				1.11
Mo	1.60	1.67	1.31	1.56	1.06	1.11	1.02	1.07
Ni					0.77	0.69	0.58	0.75

contents in weight percent are presented in Table S1 of the Supporting Information). The Ti and Zr concentrations were around 7.5 wt % for MoS_2 and around 6 wt % for Ni-MoS_2. All catalysts have comparable Mo and Ni contents: 1.39−1.65 mol % of Mo for MoS_2, as well as 1.0−1.12 and 0.61−0.78 mol % of Mo and Ni for Ni-MoS_2. The Ni/(Ni + Mo) molar ratio was around 0.4 in all NiMo catalysts. The S-to-Mo molar ratio of all Mo-containing catalysts is above 2 (2.1−2.8), possibly because of the presence of overstoichiometric sulfur.[29] The sulfur-to-metal (Ni + Mo) molar ratios of the NiMo catalysts were in the range of 1.56−1.64.

The textural properties of the catalysts are summarized in Table 2, whereas the isotherms of N_2 physisorption are presented in Figure 1. The textural properties of the supports and corresponding N_2 physisorption isotherms are presented in Table S2 and Figure S1 of the Supporting Information. The large decrease in the BET surface areas and the changes in the N_2 adsorption hysteresis suggest preferential deposition of Ti and Zr species in the pore mouth and significant differences between external and internal pore diameters. Compared with the SBA-15 support, the Mo catalysts exhibited a lower pore volume. The incorporation of Ni decreased the pore size of the catalysts, but to a lower extent compared with Mo deposition.

The X-ray diffractograms of MoS_2 and Ni-MoS_2 catalysts are presented in Figure 2. The MoS_2/Al_2O_3 catalyst exhibited reflections corresponding to γ-Al_2O_3 and weak reflections ascribed to MoS_2 (PDF: 00-024-0513) overlapping with those of the support. The MoS_2 catalysts supported on SBA-15 exhibited the broad signal around 22° 2θ typical for amorphous silica and diverse reflections for MoS_2. The number and intensity of the reflections assigned to MoS_2 suggest a higher dispersion of the sulfide phase on SBA-15 than on Zr-SBA and Ti-SBA. In Ni-MoS_2 catalysts, the only crystalline species detected was MoS_2 (and γ-Al_2O_3 from the support in Ni-MoS_2/Al_2O_3). However, variation of the intensity of the XRD reflections, relative to MoS_2 catalysts, indicated morphological changes of the MoS_2 phase induced by Ni, that is, the intensity

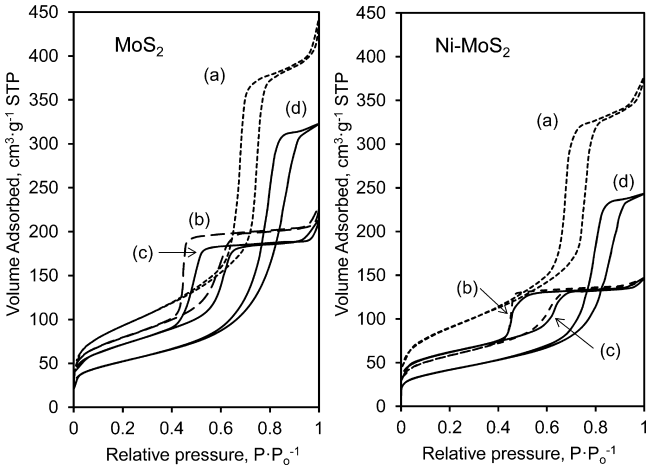

Figure 1. N_2-physisorption isotherms of MoS_2 (left) and Ni-MoS_2 (right) catalysts supported on SBA-15 (a), Ti-SBA (b), Zr-SBA (c), and Al_2O_3 (d).

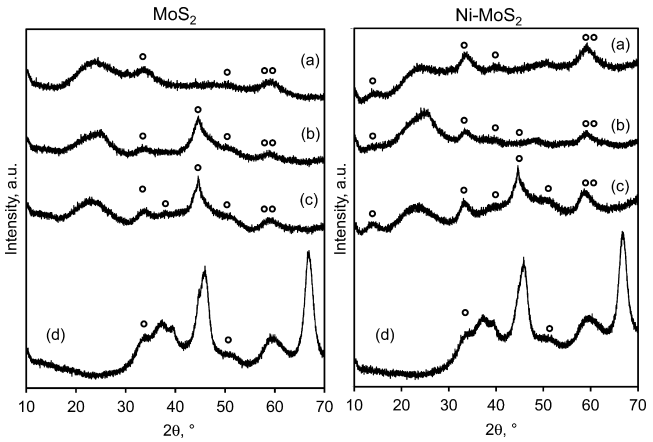

Figure 2. X-ray diffraction patterns of MoS_2 (left) and Ni-MoS_2 (right) catalysts supported on SBA-15 (a), Ti-SBA (b), Zr-SBA (c), and Al_2O_3 (d). The reflections marked with a degree sign correspond to MoS_2. The reflections in part d that are not labeled correspond to Al_2O_3.

of the signal at 44.5° 2θ decreased, and new signals were observed at 14.4° 2θ and 39.5° 2θ. The width of the reflections did not allow for a quantitative analysis of the observed changes. The reflection at 14.4° 2θ, corresponding to the (002) plane, suggests, however, that the MoS_2 crystals have more stacked layers in the promoted catalysts than in the MoS_2 counterparts.

Distribution of the stacking degree and the length of the MoS_2 particles in all catalysts were determined from the analysis of the TEM micrographs. The distributions, average, and standard deviation values are presented in Figures S2 and S3 of the Supporting Information. The average values, as well as

Table 2. Textural Properties of MoS_2 and Ni-MoS_2 Catalysts

	MoS_2 catalysts				Ni-MoS_2 catalysts			
support →	Al_2O_3	SBA-15	Ti-SBA	Zr-SBA	Al_2O_3	SBA-15	Ti-SBA	Zr-SBA
surface area, $m^2 \cdot g^{-1}$	185	334	284	254	149	322	218	224
pore vol, $cm^3 \cdot g^{-1}$	0.486	0.614	0.319	0.295	0.367	0.529	0.215	0.209
micropore vol, $cm^3 \cdot g^{-1}$	0.008	0.024	0.016	0.018	0.005	0.011	0.015	0.014
av pore diam, nm	9.5	3.3	1.8	1.9	4.9	3.2	1.7	1.8

dx.doi.org/10.1021/cs500034d | ACS Catal. 2014, 4, 1487−1499

Table 3. Morphology[a] of the MoS_2 Particles in MoS_2 and Ni-MoS_2 Catalysts and Concentration of Adsorbed NO[b]

	MoS_2 catalysts				Ni-MoS_2 catalysts			
support →	Al_2O_3	SBA-15	Ti-SBA	Zr-SBA	Al_2O_3	SBA-15	Ti-SBA	Zr-SBA
length, nm	7.2	5.6	6.3	7.0	4.4	5.6	4.7	5.4
stacking degree	1.6	3.7	2.8	2.4	1.8	3.7	2.7	3.6
f	0.17	0.22	0.18	0.17	0.27	0.22	0.26	0.22
NO adsorbed, μmol·g^{-1}	150	101	262	210	294	151	290	240

[a]Determined from TEM: average stacking degree, length and fraction of Mo atoms at the edges of the MoS_2 particles (*f*). [b]Determined by pulse experiments.

the fraction of Mo atoms at the edges of the MoS_2 particles (f), calculated according to refs 30 and 31, are summarized in Table 3. This table also reports the amount of NO adsorbed on each material. The values indicate that the concentration of adsorption sites in the presence and absence of Ni is influenced by the nature of the support.

The IR spectrum of CO adsorbed on MoS_2/Al_2O_3 (Figure 3) has four components assigned to CO adsorbed on Lewis acid sites (2197 cm^{-1}); hydroxyl groups (2156 cm^{-1}), Mo_{6c} (6-fold coordinated Mo cations) in the metal edge of the MoS_2 slabs (2114 cm^{-1}), and Mo_{6c} in the sulfur edge of the MoS_2 phase (2068 cm^{-1}).[32,33] The spectrum of CO adsorbed on SBA-15 (Figure 3) exhibits three bands at 2156, 2114, and 2070 cm^{-1}, assigned to CO adsorbed on SiOH groups, Mo_{6c} in the metal, and Mo_{6c} in the sulfur edge of the MoS_2 phase, respectively. The Ti and Zr surface modification of the SBA-15 material induced Lewis acidity, as evidenced by the bands at 2184 and 2188 cm^{-1} for MoS_2/Ti-SBA and MoS_2/Zr-SBA, respectively. These Lewis sites (presumably Ti^{4+} and Zr^{4+}) are weaker than those in Al_2O_3, as concluded from the higher wavenumber of the stretching vibrations (ν(CO)) on the latter.[34] For the sake of clarity, Figure 4 (left) presents the above-described assignments for the spectrum of CO adsorbed on MoS_2/Al_2O_3.

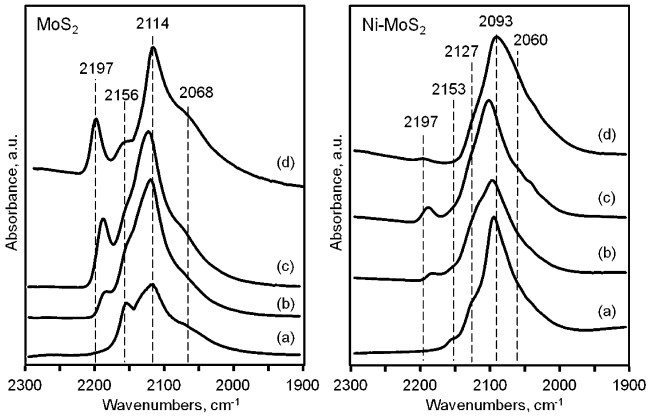

Figure 3. IR spectra of CO adsorbed on MoS_2 (left) and Ni-MoS_2 (right) catalysts supported on SBA-15 (a), Ti-SBA (b), Zr-SBA (c), and Al_2O_3 (d).

The IR spectra of CO adsorbed on the series of Ni-MoS_2 catalysts are shown in Figure 3. All spectra had at least five bands, most of them overlapping. In the catalysts supported on Al_2O_3, Zr-SBA, and Ti-SBA, the bands at 2197, 2189, and 2178 cm^{-1}, respectively, correspond to CO adsorbed on Lewis sites. The low-intensity band at 2153 cm^{-1} in all spectra is attributed to CO adsorbed on OH groups. The shoulder at 2124, 2123, 2128, and 2125 cm^{-1} on the sulfide supported on SBA-15, Zr-SBA, Ti-SBA, and Al_2O_3, respectively, is assigned to CO adsorbed on Ni atoms on the edges of the promoted MoS_2 crystals.[35] The main band, at 2096, 2097, 2103, and 2110 cm^{-1} (on SBA-15, Zr-SBA, Ti-SBA, and Al_2O_3, respectively) is attributed to CO adsorbed on Mo_{6c} sites. The shoulder at 2075−2084 cm^{-1} is attributed to the adsorption of CO on 5-fold-coordinated Mo sites in the vicinity of the Ni atom promoter. Finally, the adsorption bands at lower wavenumbers are attributed to Mo sites of varying coordination in the promoted phase or segregated nickel sulfide phases. Figure 4

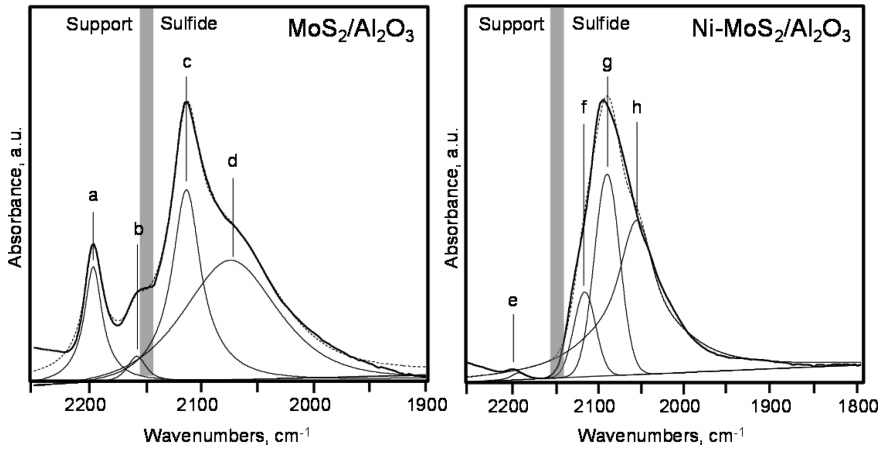

Figure 4. Assignment of the deconvoluted bands of the IR spectra of CO adsorbed on MoS_2/Al_2O_3 (left) and Ni-MoS_2/Al_2O_3 (right): CO on Brønsted sites on the support (a); CO on Lewis acid sites on the support (b); CO on Mo cations at the metal edge of MoS_2 (c); CO on Mo cations at the sulfur edge of the MoS_2 phase (d); CO on Brønsted sites on the support (e); CO on Ni cations at the edges of MoS_2 (f); CO on Mo cations (g); and CO on Mo sites in the vicinity of Ni cations (h).

dx.doi.org/10.1021/cs500034d | ACS Catal. 2014, 4, 1487−1499

(right) illustrates the assignments of the bands of CO adsorbed on support and MoS_2 for Ni-MoS_2/Al_2O_3.

The intensities of bands corresponding to CO adsorbed on acid sites (Lewis acid sites and hydroxyl groups) of promoted catalysts decrease significantly compared with the nonpromoted catalysts. This observation confirms the rearrangement of the sulfide phase suggested by XRD, NO adsorption, and TEM analysis. Figure 4 illustrates the deconvolution of the IR spectra of CO adsorbed on MoS_2/Al_2O_3 and Ni-MoS_2/Al_2O_3 to evidence the goodness of fit. The results of the deconvolution of all spectra are presented in the Supporting Information (Figures S4 and S5 and Tables S3 and S4). The areas and positions of the deconvoluted bands were used to rationalize the effects of promoter and support on HDS and HDN activities, as described in the Discussion section. It must be mentioned that the position of the bands did not appreciably vary as a function of the CO pressure below the equilibrium value of 1 mbar, as illustrated in Supporting Information (Figure S6) for Ni-MoS_2 catalysts.

Activity of the Mo Catalysts. The conversions of DBT and OPA on MoS_2 catalysts are shown in Figure 5. The trend

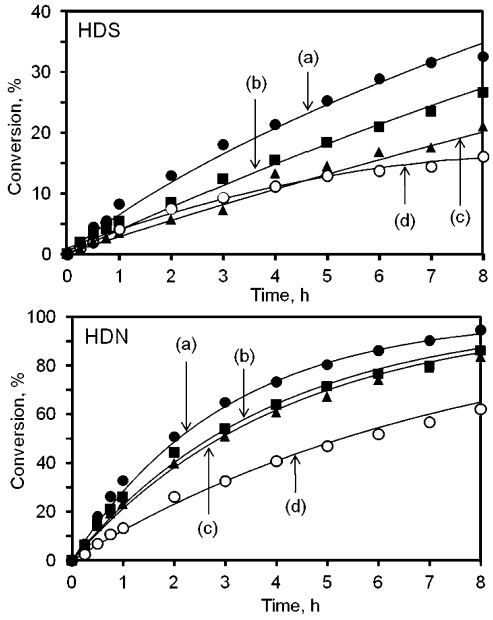

Figure 5. Conversion of dibenzothiophene (hydrodesulfurization, HDS) and *o*-propylaniline (hydrodenitrogenation, HDN) MoS_2 catalysts supported on SBA-15 (a), Ti-SBA (b), Zr-SBA (c), and Al_2O_3 (d).

lines shown are the result of the fitting procedure described below. The activities, as a function of the support, increased in the order: Al_2O_3 ~ Zr-SBA-15 < Ti-SBA-15 < SBA-15 (HDS activity), and Al_2O_3 < Zr-SBA-15 < Ti-SBA-15 < SBA-15 (HDN activity). In all cases, the HDN activity was higher than the HDS activity. The concentration profiles of reactants and products are presented in Figures S7 and S8 of the Supporting Information. The results do not suggest that the reaction networks for HDS of DBT and HDN of OPA on the catalysts studied differ from those widely accepted in literature for MoS_2-based catalysts (see for instance refs 36−45). Thus, the following kinetic analyses are based on the reaction networks presented in Figures 6 and 7. The HDS of DBT proceeds either via direct desulfurization (DDS), (k_{HDS1} in Figure 6) yielding

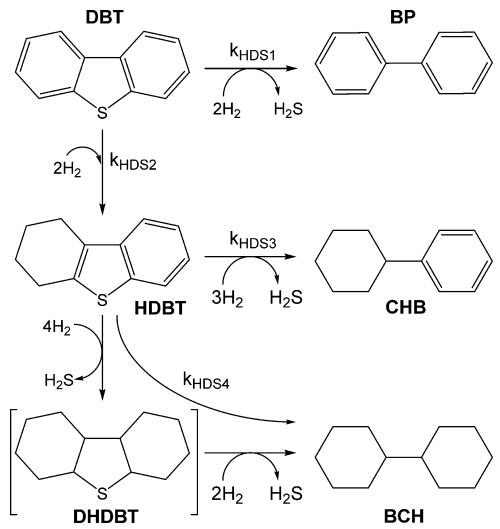

Figure 6. Reaction network for the hydrodesulfurization of dibenzothiophene. The compounds involved in the reaction network are dibenzothiophene (DBT), biphenyl (BP), tetrahydrodibenzothiophene (HDBT), cyclohexylbenzene (CHB), decahydrodibenzothiophene (DHDBT), and bicyclohexyl (BCH).

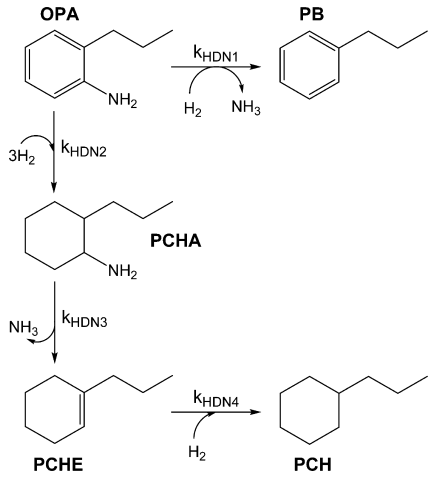

Figure 7. Reaction network for the hydrodenitrogenation of *o*-propylaniline. The compounds involved in the reaction network are *o*-propylaniline (OPA), propylbenzene (PB), propylcyclohexylamine (PCHA), 3-propylcyclohexene (PCHE), and propylcyclohexane (PCH).

biphenyl (BP) or hydrogenation (HYDS) to tetrahydrodibenzothiophene (HDBT), followed by sulfur removal to cyclohexylbenzene (CHB) (k_{HDS2} → k_{HDS3}, in Figure 6), or consecutive hydrogenation of HDBT to decahydrodibenzothiophene (DHDBT), followed by sulfur removal to bicyclohexyl (BCH). The latter steps (HDBT → DHDBT → BCH) were lumped into a single hydrodesulfurization step (k_{HDS4}) because DHDBT is too reactive to be observed.[38,39]

The HDN of OPA proceeds via two routes: direct denitrogenation (DDN), (k_{HDN1} in Figure 7) leading to propylbenzene (PB); and hydrogenation (HYDN) to propylcyclohexylamine (PCHA), with the subsequent nitrogen removal and hydrogenation to 3-propylcyclohexene (PCHE) and propylcyclohexane (PCH), respectively (for this study, PCHE represents the sum of the three isomers 1-propylcyclohexene, 3-propylcyclohexene, and propylidene cyclohexane). In Figure 7, the HDN hydrogenation route is

dx.doi.org/10.1021/cs500034d | ACS Catal. 2014, 4, 1487−1499

$k_{HDN2} \rightarrow k_{HDN3} \rightarrow k_{HDN4}$. On all the catalysts studied here, DBT was converted mainly through direct desulfurization, leading to biphenyl as the main product within the whole DBT conversion range. OPA was converted preferentially (with PCHE and PCH being the main products below and above 20% of OPA conversion, respectively) via the hydrogenation pathway, that is, OPA → PCHA → PCHE → PCH.

To quantitatively describe the trends in activity, we attempted to calculate pseudo-first-order reaction rate constants for the HDS and HDN reactions; however, preliminary fittings were not satisfactory because the reaction order in DBT and OPA seemed to be fractional, as inferred from the shape of the conversion lines. The HDS of model compounds on MoS_2 in the absence of N-containing compounds has been described with pseudo-first-order kinetics.[46,47] In this work, the severe deviation of HDS from first-order kinetics is tentatively attributed to the inhibiting effect of OPA and the products of HDN. Note that in all reactions performed on MoS_2 catalysts, two regimes in conversion were differentiated: below and above 20% of OPA conversion. Both HDN and HDS could be satisfactorily fitted to pseudo-first-order kinetics for OPA conversions below 20%. At OPA conversions higher than 20%, however, the reaction rates decreased (see the slope of the conversion curves). This effect was minor for converting OPA, but HDS was severely inhibited. These observations suggested that NH_3, formed by the denitrogenation of OPA and PCHA, is strongly adsorbed on the active sites, retarding HDS. The observation is in line with results reported for HDS and hydrogenation reactions performed in the presence of ammonia[48,49] and the strong interaction expected between the strongly basic NH_3 and the Lewis acid sites needed for DBT conversion.

To account for the competitive adsorption of products, it was decided to adjust the experimental data to the Langmuir–Hinshelwood model represented in eqs 1–9, where C_i is the concentration of the species i, and k_j is the reaction rate constant of the step j in Figures 7 and 8. It is not possible to determine the adsorption equilibrium constants of all the products from the present results; however, with the aim of quantitatively discussing the resistance of the catalysts to inhibition, the concentration of products competing in HDS of DBT was calculated as the product of the initial concentration of OPA and its conversion, whereas the concentration of products competing in OPA HDN was calculated as the product of the initial DBT concentration and its conversion. By doing this, it was explicitly assumed that the concentration of products inhibiting HDS was approximately the concentration of NH_3, whereas the concentration of products inhibiting HDN is equivalent to the concentration of H_2S. This is in agreement with the predominance of direct desulfurization in HDS, the fast denitrogenation rates, and the conclusion that NH_3 is the main inhibiting species for HDS. Hence, in eqs 1–9, K_{H_2S} and C_{H_2S} are the lumped adsorption equilibrium constants and concentration or the species competing for the active sites in HDN, whereas K_{NH_3} and C_{NH_3} are the adsorption equilibrium constants and concentration or the species competing for the active sites in HDS. It has to be noted that the effect of the relatively strong base PCHA was not taken into account because it occurs only in low concentrations (see Figures S8 and S10 in the Supporting Information). This simplification was applied to facilitate the quantification of the inhibition, although we are aware that the mutual effect of S- and N-containing compounds for HDS and HDN is complex and depends on many parameters.[50−53] Detailed kinetic models, aiming at the calculation of HDS and HDN surface reaction rate constants and adsorption constants, have been reported by several groups (see refs 54−58).

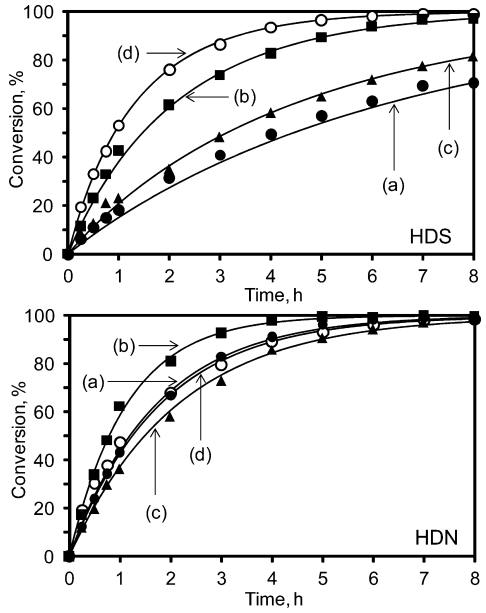

Figure 8. Conversion of dibenzothiophene (hydrodesulfurization, HDS) and *o*-propylaniline (hydrodenitrogenation, HDN) Ni-MoS_2 catalysts supported on SBA-15 (a), Ti-SBA (b), Zr-SBA (c), and Al_2O_3 (d).

$$\frac{dC_{DBT}}{dt} = \frac{-(k_{HDS1} + k_{HDS2})C_{DBT}}{1 + \sum K_{NH_3}C_{NH_3}} \quad (1)$$

$$\frac{dC_{BP}}{dt} = \frac{k_{HDS1}C_{DBT}}{1 + \sum K_{NH_3}C_{NH_3}} \quad (2)$$

$$\frac{dC_{HDBT}}{dt} = \frac{k_{HDS2}C_{DBT}}{1 + \sum K_{NH_3}C_{NH_3}} - \frac{k_{HDS3}C_{HDBT}}{1 + \sum K_{NH_3}C_{NH_3}} - \frac{k_{HDS4}C_{HDBT}}{1 + \sum K_{NH_3}C_{NH_3}} \quad (3)$$

$$\frac{dC_{CHB}}{dt} = \frac{k_{HDS3}C_{HDBT}}{1 + \sum K_{NH_3}C_{NH_3}} \quad (4)$$

$$\frac{dC_{OPA}}{dt} = \frac{-(k_{HDN1} + k_{HDN2})C_{OPA}}{1 + \sum K_{H_2S}C_{H_2S}} \quad (5)$$

$$\frac{dC_{PB}}{dt} = \frac{k_{HDN1}OPA}{1 + \sum K_{H_2S}C_{H_2S}} \quad (6)$$

$$\frac{dC_{PCHA}}{dt} = \frac{k_{HDN2}C_{OPA}}{1 + \sum K_{H_2S}C_{H_2S}} - \frac{k_{HDN3}C_{PCHA}}{1 + \sum K_{H_2S}C_{H_2S}} \quad (7)$$

$$\frac{dC_{PCHE}}{dt} = \frac{k_{HDN3}C_{PCHA}}{1 + \sum K_{H_2S}C_{H_2S}} - \frac{k_{HDN4}C_{PCHE}}{1 + \sum K_{H_2S}C_{H_2S}} \quad (8)$$

$$\frac{dC_{PCH}}{dt} = \frac{k_{HDN4}C_{PCHE}}{1 + \sum K_{H_2S}C_{H_2S}} \quad (9)$$

dx.doi.org/10.1021/cs500034d | ACS Catal. 2014, 4, 1487−1499

The overall rate constants for HDS ($k_{HDS1} + k_{HDS2}$; see Table 4) are in line with the activity trend exhibited by the DBT

Table 4. First-Order Reaction Rate Constants, k_i ($\times 10^{-2}$ mol·h^{-1}·L^{-1}) for the Hydrodesulfurization (HDS) of Dibenzothiophene[a] and Overall Adsorption Constants of Compounds Competing for HDS sites, K_{NH_3}, on MoS_2 Catalysts

	k_{HDS1}	k_{HDS2}	k_{HDS3}	$k_{HDS1} + k_{HDS2}$	k_{HDS1}/k_{HDS2}	K_{NH_3}
MoS_2/Al_2O_3	4.9	0.07	0.22	5.0	76	167
MoS_2/SBA	7.4	0.15	0.30	7.6	48	90
MoS_2/Ti-SBA	6.0	0.08	0.13	6.1	72	120
MoS_2/Zr-SBA	4.7	0.10	0.28	4.8	53	130

[a]See Figure 6 for the reaction network.

conversions, that is, the activity increases in the function of the support in the order Zr-SBA < Al_2O_3 < Ti-SBA-15 < SBA-15. The direct desulfurization pathway by far dominates HDS, and as a consequence, the trend of the k_{HDS1} values is identical to that of the overall reactivity. In all cases, the rate constants of the hydrogenating step (k_{HDS2}) are orders of magnitude lower than those of the direct desulfurization (k_{HDS1}) and lead to k_{HDS1}/k_{HDS2} ratios from 48 to 76. The hydrogenation of DBT (k_{HDS2}) on MoS_2 catalysts supported on SBA and Zr-SBA is faster than on MoS_2 supported on Al_2O_3 and Ti-SBA. The suppression of the hydrogenation route and concomitant large preference for the direct sulfur removal pathway in HDS may be due to the competitive adsorption of OPA on hydrogenation sites. In the absence of N-containing compounds, similar supported MoS_2 systems do not favor direct desulfurization over hydrogenation to such a large extent.[59,60]

The overall OPA HDN constants ($k_{HDN1} + k_{HDN2}$; see Table 5) also followed the described OPA conversion trends; that is,

Table 5. First-Order Reaction Rate Constants, k_i (x 10^{-2} mol·h^{-1}·L^{-1}), for the Hydrodenitrogenation of *o*-Propylaniline[a] on MoS_2 Catalysts

	k_{HDN1}	k_{HDN2}	k_{HDN3}	k_{HDN4}	$k_{HDN1} + k_{HDN2}$	k_{HDN2}/k_{HDN1}
MoS_2/Al_2O_3	4.2	8.9	15 700	69	13.2	2.1
MoS_2/SBA	9.0	22.0	36 700	105	31.0	2.5
MoS_2/Ti-SBA	6.6	21.0	60 200	105	27.6	3.2
MoS_2/Zr-SBA	7.3	15.9	41 900	91	23.2	2.2

[a]See Figure 7 for the reaction network.

the activity increased in the order Al_2O_3 < Zr-SBA-15 < Ti-SBA-15 < SBA-15 support. The k_{HDN2}/k_{HDN1} ratios showed that the HDN hydrogenation route was 2.1−3.2 times faster than the direct nitrogen removal. The NH_3 elimination from PCHA (k_{HDN3}) was several orders of magnitude faster than the other HDN steps. The values of k_{HDN1}, k_{HDN2}, and k_{HDN4} followed trends similar to that of the overall activity, whereas the values of k_{HDN4} were similar on all MoS_2 catalysts.

The values of the lumped adsorption equilibrium constants of the compounds inhibiting HDN (K_{H_2S}) were negligible; for example, on the order of 10^{-7}. In contrast, the lumped adsorption equilibrium constants of the products inhibiting the HDS were very significant, as seen in Table 4. The product inhibition of HDS increases in the order (in function of the support) SBA-15 < Ti-SBA < Zr-SBA < Al_2O_3.

Activity of the NiMo Catalysts. The activity of the Ni-promoted catalysts was much higher than that of the MoS_2 catalysts (Figure 8); however, the extent of promotion depended on the support composition because the activity trends differed from those observed for MoS_2 catalysts. The activities, in function of the support, increased in the sequence SBA-15 < Zr-SBA-15 < Ti-SBA-15 < Al_2O_3, and Zr-SBA-15 < Al_2O_3 < SBA-15 < Ti-SBA-15 for HDS and HDN, respectively. The HDN rates were higher than the HDS rates with the exception of Ni-MoS_2/Al_2O_3. The concentration profiles of reactants and products are presented in Figures S9 and S10 of the Supporting Information.

The rate constants of the reaction network of DBT HDS and OPA HDN on Ni-MoS_2 catalysts are presented in Tables 6 and

Table 6. First-Order Reaction Rate Constants, k_i ($\times 10^{-2}$ mol·h^{-1}·L^{-1}), for the Hydrodesulfurization of Dibenzothiophene[a] and Overall Adsorption Constants of Compounds Competing for HDS Sites, K_{NH_3}, on Ni-MoS_2 Catalysts

	k_{HDS1}	k_{HDS2}	k_{HDS3}	k_{HDS4}	$k_{HDS1} + k_{HDS2}$	k_{HDS1}/k_{HDS2}	K_{NH_3}
Ni-MoS_2/Al_2O_3	80.7	0.20	3.8	1.3	80.9	396	12
Ni-MoS_2/SBA	18.1	0.34	5.2	1.1	18.5	54	4
Ni-MoS_2/Ti-SBA	50.2	0.27	2.5	1.1	50.5	183	6
Ni-MoS_2/Zr-SBA	24.0	0.16	6.1	1.2	24.2	149	8

[a]See Figure 6 for the reaction network.

Table 7. First-Order Reaction Rate Constants, k_i ($\times 10^{-2}$ mol·h^{-1}·L^{-1}), for the Hydrodenitrogenation of Propylaniline[a] on Ni-MoS_2 Catalysts

	k_{HDN1}	k_{HDN2}	k_{HDN3}	k_{HDN4}	$k_{HDN1} + k_{HDN2}$	k_{HDN2}/k_{HDN1}
Ni-MoS_2/Al_2O_3	2.1	53.4	46 000	416	56	25
Ni-MoS_2/SBA	4.8	53.4	55 500	131	58	11
Ni-MoS_2/Ti-SBA	3.8	84.5	76 100	339	88	22
Ni-MoS_2/Zr-SBA	3.5	46.7	42 000	135	50	13

[a]See Figure 7 for the reaction network.

7. The trends of the overall HDS and HDN rate constants ($k_{HDS1} + k_{HDS2}$, and $k_{HDN1} + k_{HDN2}$, respectively) were the same as those described for reactant conversions. As with MoS_2, a remarkable preference for the direct desulfurization of DBT and hydrogenation of OPA was observed via the concentrations of BP in HDS and PCHE (or PCH) in HDN. Moreover, a non-negligible concentration of BCH was detected during the HDS of DBT. The experimental data obtained on Ni-MoS_2 catalysts could be satisfactorily adjusted to first-order kinetics; however, to be able to discuss the effect of Ni and to compare the performance of MoS_2 and Ni-MoS_2 catalysts, the reaction rate constants of all steps were calculated using the same simplified Langmuir−Hinshelwood model described above.

dx.doi.org/10.1021/cs500034d | ACS Catal. 2014, 4, 1487−1499

All the HDS reaction constants increased with the Ni promotion, however, not to the same extent. This produced trends that were different from those observed for MoS_2. The values of k_{HDS1} increased twice for the catalysts supported on Zr-SBA and SBA-15, respectively, whereas on Al_2O_3 and Ti-SBA, k_{HDS1} increased 17 and 8 times, respectively. The same behavior was observed for k_{HDS2} that increased more than three times on Al_2O_3 and Ti-SBA, but only twice on Zr-SBA and SBA-15. Hence, the catalysts supported on Al_2O_3 and Ti-SBA were the most active for HDS of DBT, although those supported on SBA-15 and Zr-SBA maintain higher activity for hydrogenation. The direct sulfur removal was more favored than the hydrogenation pathway by the Ni promotion. As a result, the k_{HDS1}/k_{HDS2} ratios on the Ni-MoS_2 catalysts are higher than those calculated for MoS_2.

In the OPA HDN reaction network, all the rate constants increased with Ni promotion, with the notable exception of k_{HDN1}, which decreased. The interplay between the lower k_{HDN1} and the higher k_{HDN2} values yielded different activity trends and higher k_{HDN2}/k_{HDN1} ratios compared with those observed for MoS_2 catalysts. The N-elimination rate from PCHA increased on SBA-type materials in a similar proportion (around 1.5 times), somewhat less than on alumina (3 times). The values of k_{HDN4} also increased more on Al_2O_3 and Ti-SBA than on SBA-15 and Zr-SBA.

Interestingly, the lumped adsorption equilibrium constants of the inhibiting products calculated on Ni-MoS_2 catalysts are lower than those on MoS_2 (Table 6), that is, the products were less strongly adsorbed on Ni-MoS_2 than on MoS_2. The K_{H_2S} (adsorption of products inhibiting HDN) values were in the order of 10^{-7} and, therefore, neglected as in the case of the MoS_2 catalysts. The K_{NH_3} (adsorption of products inhibiting HDS) values for Ni-MoS_2 catalysts were 1 order of magnitude lower than those of the unpromoted counterparts following the sequence SBA-15 < Ti-SBA < Zr-SBA < Al_2O_3.

DISCUSSION

On the Active Sites for HDS and HDN. It has been accepted that the catalytically active sites in nonpromoted and Ni(Co)-promoted MoS_2 are located at the edges of the slabs, where coordinatively unsaturated sites (CUS), that is, exposed Mo (or promoter) cations, exist.[61,62] The basal planes are considered largely unreactive. The different actions of the catalysts, that is, direct heteroatom removal or hydrogenation, have been rationalized as sites formed with a varying number of adjacent CUS and neighboring hydrogen atoms.[39,63] Interestingly, even fully sulfided MoS_2 edges have been claimed to be active sites for hydrogenolysis, for example, ring-opening of N-containing compounds.[56,64] In addition, the structure of MoS_2 has been proven to be a determining factor for the conversion of bulky compounds. For instance, the well-known rim-edge model proposes that desulfurization of dibenzothiophenic compounds occurs on all slabs of a MoS_2 stack (edges and rims), whereas hydrogenation is limited to the top and bottom slabs (rims).[65] The hydrogenation functionality of the catalysts has also been correlated with corners, where the expected higher probability for the formation of adjacent vacancies should lead to higher reactivity.[66,67] Sterically hindered compounds, on the other hand, may have problems to access the active sites in the MoS_2 slabs in the proximity of the support.[30,60,68] Some structural models also attempt to define different sites for hydrogenation of aromatic compounds and alkenes.[69]

The controversies concerning the description of the active sites in Mo-based sulfide catalysts have been intensified in recent years with the postulate of the "brim sites". These sites are described as metal-like regions located near the edges of the sulfide slabs that are able to catalyze hydrogenation and C−S bond cleavage.[70,71] In recent works, brim sites have also been correlated with the adsorption of N-containing model molecules.[72]

Similarly to our results (discussed below), the presence of N-containing aromatic compounds has been found to suppress the hydrogenation pathways in hydrodesulfurization of model compounds and real feeds.[73−75] Furthermore, N-containing compounds strongly inhibit hydrogenation of aromatic compounds, which also links HDN with hydrodearomatization.[76,77] In contrast, the presence of S-containing compounds has been found to have no effect or an enhancing one on the hydrogenation rates of HDN.[41,56,73,74,78] As for the C−S and C−N cleavage functionalities, hydrogenolitic pathways are considered to share the same active sites (CUS), whereas N-removal, via, for example, Hoffman type elimination, is concluded to occur on acidic SH groups.[36,52,77]

The adsorption of dibenzothiophenic compounds on CUS has been concluded to occur in a plug-in mode through electron donation of the S atom for direct sulfur removal. In contrast, hydrogenation requires a flat adsorption resulting from the donation of π-electrons from the aromatic ring to the active site.[79,80] The adsorption geometry (flat, leading to hydrogenation) would not change on brim sites, as suggested recently.[81] Therefore, regardless of the nature of the active sites, the adsorption mode of the reactant molecules may dictate the favored reaction pathway in HDS and the effect of competitive interactions. OPA and DBT can adsorb via a benzenic ring or heteroatom and, therefore, may compete for the same sites.

The direct removal of S and N atoms is very likely to proceed on CUS via a reverse Mars−van Krevelen mechanism[39,41,82] (correlations between DDS and DDN with CUS are shown below). Evidence of CUS as active sites for direct desulfurization is the strong effect of NH_3 (high K_{NH_3} values) on the HDS of DBT. On promoted catalysts, the NH_3 poisoning effect remains, although it decreases by 1 order of magnitude due to accelerated C−S bond cleavage.

In contrast to the convention on the nature of active sites for direct S- and N-removal steps (CUS), the hydrogenation sites are under strong debate. OPA suppresses the hydrogenation steps of the HDS network (vide supra), suggesting that OPA and dibenzothiophenic compounds share the same sites for parallel adsorption. In contrast, DBT has little influence on the hydrogenation sites of OPA.[41] Furthermore, the OPA HDN is largely insensitive to the increasing concentration of H_2S or NH_3, known to adsorb on CUS. All this indicates that there are two kinds of sites that lead to hydrogenation: one is accessible only to OPA, whereas the second is accessible for OPA and DBT. In turn, NH_3 produced during HDN adsorbs strongly on the sites for DBT conversion.

In the classical view, the hydrogenation of aromatic rings may occur on adjacent CUS.[39,67,69] In this case, the size of the molecules should dictate their accessibility to CUS, that is, OPA, with a single aromatic ring, would require less space to adsorb than the relatively bulky DBT. Therefore, the hydrogenation of OPA is not affected by DBT to the extent

Table 8. Turnover Frequency Values for the HDN of OPA and HDS of DBT on MoS_2 Catalysts Calculated from the Corresponding Reaction Rate Constants[a] and the Fraction of Mo Atoms at the Edges of the MoS_2 Particles, f (a); the Concentration of NO Adsorbed during Pulse Experiments (b); and the Sum of the Integrated Areas of the Deconvoluted Peaks of the CO-IR Spectra (c)

	HDS			HDN		
support	(a) f, h^{-1}	(b) NO, $mol^{-1}\cdot s^{-1}$	(c) CO, h^{-1}	(a) f, h^{-1}	(b) NO, $mol^{-1}\cdot s^{-1}$	(c) CO, h^{-1}
Al_2O_3	0.29	0.37	0.0037	0.77	0.97	0.009
SBA-15	0.35	0.83	0.0088	14.1	3.41	0.036
Ti-SBA	0.34	0.26	0.0045	15.3	1.17	0.020
Zr-SBA	0.28	0.25	0.0033	13.6	1.22	0.016

[a] $k_{HDS1} + k_{HDS2}$, $k_{HDN1} + k_{HDN2}$; see Tables 4 and 5.

Table 9. Turnover Frequency Values for the HDN of OPA and HDS of DBT on Ni-MoS_2 Catalysts Calculated from the Corresponding Reaction Rate Constants[a] and the Fraction of Mo Atoms at the Edges of the MoS_2 Particles, f (a); the Concentration of NO Adsorbed during Pulse Experiments (b); and the Sum of the Integrated Areas of the Deconvoluted Peaks of CO-IR Spectra (c)

	HDS			HDN		
support	(a) f, h^{-1}	(b) NO, $mol^{-1}\cdot s^{-1}$	(c) CO, h^{-1}	(a) f, h^{-1}	(b) NO, $mol^{-1}\cdot s^{-1}$	(c) CO, h^{-1}
Al_2O_3	3.0	3.06	0.043	20.6	2.10	0.029
SBA-15	0.84	1.36	0.012	26.5	2.48	0.038
Ti-SBA	1.94	1.93	0.038	34.0	3.38	0.066
Zr-SBA	1.10	1.12	0.015	22.8	2.32	0.030

[a] $k_{HDS1} + k_{HDS2}$, $k_{HDN1} + k_{HDN2}$; see Tables 6 and 7.

that the hydrogenation of DBT is hindered by OPA. However, the null effect of NH_3 on the conversion of OPA speaks against steric effects (because NH_3 is much smaller than OPA or DBT). It may be that whereas OPA and DBT adsorb on CUS (parallel and normal to the surface), OPA also adsorbs and hydrogenates on brim sites as it is suggested by recent studies that N-containing compounds adsorb and hydrogenate on brim sites.[40,72,81] At present, we speculate that the hydrogenation of OPA occurs on CUS and brim sites in view of the weak effect of the HDN and HDS reaction products (because H_2S and NH_3 must adsorb preferentially on CUS) on the OPA HDN and the lack of correlation between CUS and OPA hydrogenation (vide infra). Alternatively, other authors have associated CUS with hydrogenolysis and hydrogenation and sulfur-saturated sites with hydrogenation.[77]

In some works, the concentration of CUS, determined by titration with probe molecules, has been satisfactorily correlated with the activity of MoS_2 catalysts.[83−86] In stark contrast, in other studies, the concentration of sites adsorbing probe molecules does not satisfactorily correlate catalytic activity.[87−89] This is probably due to the reactivity of the probes with the sulfide surface, varying intrinsic reactivity (due to the presence of promoters of incomplete sulfidation), or the higher steric constraints of reactants compared with the probe molecule to the active sites.

Here, the concentration of CUS was analyzed by titrating the sulfides with two probes, that is, NO at room temperature (pulse experiments) and CO at 128 K. Unfortunately, it is not possible to correlate the concentration of adsorbed probe molecules and the activity of the MoS_2 catalysts. A correlation exists, however, between the dispersion of the MoS_2 phase determined by TEM and the rate constants of the overall conversion of DBT and OPA. Comparing the f values (fraction of Mo atoms at the edges of MoS_2 crystals) presented in Table 3 and the ($k_{HDS1} + k_{HDS2}$) and ($k_{HDN1} + k_{HDN2}$) values for MoS_2 catalysts (Tables 4 and 5), the same trends arise. Thus, increasing dispersion of the active surface increases the activity of the catalysts, regardless the nature of the active sites. In this respect, it is clear that the support providing the highest dispersion to the MoS_2 phase leads to the highest activity.

To our surprise, the trends in concentrations of chemisorbed NO (volumetric experiments), chemisorbed CO (followed by IR spectroscopy), and f values (derived from TEM measurements) are not the same within the series of catalysts. We used the data, however, to determine turnover frequencies for HDS of DBT and HDN of OPA to explore the possibility of normalizing catalytic activity using those methods. Tables 8 and 9 present the turnover frequency values for HDS and HDN on MoS_2 and Ni-MoS_2 catalysts. The trends of all TOF values are the same as those observed for the corresponding conversions and reaction rate constants (Figures 5 and 8 and Tables 4−7). Tables S6−S11 of the Supporting Information report the TOF values for particular pathways, that is, desulfurization, denitrogenation, and hydrogenation. The trends of these particular TOF values are also similar to those observed for the corresponding reaction rate constants.

One might expect similar TOFs within the series of MoS_2 or Ni-MoS_2 catalysts; however, that would be reasonably expected only if the active phase (or the active sites dominating the activity) in all catalysts has the same sulfidation and promotion degrees and support effect. This condition is definitively not met in the series of catalysts used in this work as discussed below; therefore, largely differing TOF values were obtained. In turn, similar trends in overall activity and TOF values suggest that the overall activity is governed by the intrinsic activity of the catalysts.

We attribute the mismatch among trends of activity and concentrations of adsorbed NO and CO to differences in the nature of the information provided by the characterization techniques. It is possible that CO unselectively titrates sites at the edges with different coordinations,[32,33] whereas NO titrates CUS and may also remove sulfur at the edges through push−

dx.doi.org/10.1021/cs500034d | ACS Catal. 2014, 4, 1487−1499

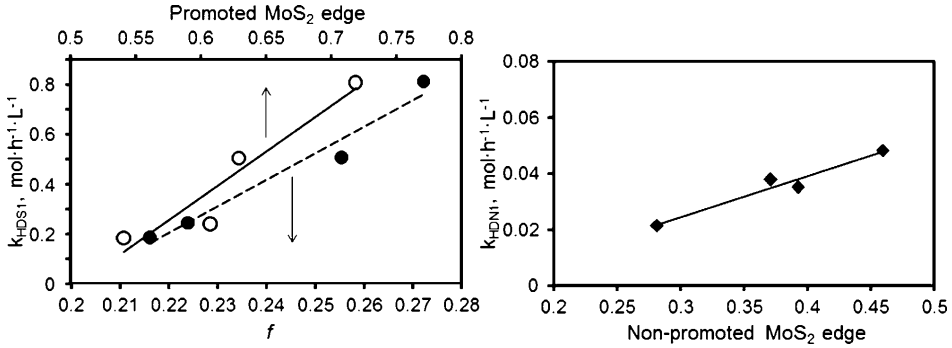

Figure 9. Left: correlations between k_{HDS1} (see Figure 6) and f (see Table 3) and the fraction of promoted edge in the Ni-MoS_2 catalysts. Right: correlation between k_{HDN1} (see Figure 7) and the fraction of nonpromoted MoS_2 edge in the Ni-MoS_2 catalysts.

pull type mechanisms.[90] The values of f, on the other hand, summarize purely structural information provided by TEM measurements. Evidently, these techniques may be measuring different properties of the sulfide phase, that is, surface structure (CO adsorption), reactivity toward oxidation (NO adsorption), and dispersion (f). With these considerations, it is no longer surprising that those techniques exhibit different trends and that they correlate with catalytic activity only in relatively few studies focused on the conversion of model sulfur-containing compounds.[60,83,91] Hence, although CO- and NO-chemisorption experiments provide insightful information on the structure and surface of the sulfide materials, these techniques do not seem suitable for the quantification of the sites active during simultaneous processes (HDS, HDN) or for quantitative comparison among catalysts subjected to very different promoter and support effects.

Effect of the Promoter. The addition of Ni increases the dispersion of the MoS_2 phase (according to the increase in the f values) and the concentration of adsorption sites (NO and CO adsorption experiments). However, the increase in HDS (DDS and HYDS routes) and DDN activity is much larger than that of dispersion or adsorption capacity of the MoS_2 phase. Therefore, we conclude that the active sites created with the addition of Ni are intrinsically much more active than those in the nonpromoted catalysts. This suggests that the addition of Ni leads to the formation of the Ni−Mo−S phase, which is much more active than phase-pure MoS_2.[92,93] In this Ni-promoted phase, Ni substitutes Mo cations at the perimeter of the MoS_2 slabs and, therefore, is also referred to as a decoration model. This improvement in the activity and concentration of active sites must be the cause of the notable decrease of poisoning of HDS by ammonia (the K_{NH_3} for Ni-MoS_2 catalysts are 1 order of magnitude smaller than those of MoS_2 catalysts).

In HDS, the DDS pathway is more enhanced than the HYDS pathway in line with previous observations that the rate of C−S bond cleavage is enhanced with the addition of Ni.[39] Similarly, the sulfur removal from HDBT (k_{HDS3}) is accelerated to a large extent with Ni promotion. The values of k_{HDS1} increase in the same fashion as the dispersion determined by NO adsorption and TEM (the correlation between k_{HDS1} and f is shown in Figure 9). This indicates that the Ni−Mo−S phase dominates the activity on all the supports. However, not all catalysts have identical decoration, and the k_{HDS1} values correlate with the fraction of promoted MoS_2 edge calculated from the deconvoluted IR-CO adsorption spectra (see Table S5 of the Supporting Information). The linear correlation between k_{HDS1} and the fraction of promoted edge (Figure 9) indicates that at least two CUS are needed to perform the C−S bond cleavage: a S vacancy on Mo and another on Ni. Other groups have also concluded the need for two vacancies to perform the direct desulfurization.[39] That is, one vacancy to bind and retain the sulfur atoms and another one to adsorb the hydrogenated intermediate. In turn, the lineal correlation between k_{HDS1} and the fraction of promoted edge explains the change in HDS activity trends comparing MoS_2 and Ni-MoS_2 catalysts. That is, enhancing the promoter effect overcomes the importance of the dispersion of the parent unpromoted MoS_2 phase.

The hydrogenation step of DBT HDS (k_{HDS2}) was also accelerated with the Ni promotion. It is difficult to discuss the differences in k_{HDS2} among the catalysts because of the low values and the competitive adsorption of N-containing compounds. However, we also observe that the catalysts exhibiting the MoS_2 slabs with the highest average stacking degree (those supported on SBA-15 and Zr-SBA, as seen in Table 3) exhibited the highest hydrogenation rates in HDS.[60,94]

In HDN, the effect of Ni is more complex than in HDS because not all reaction pathways are accelerated by promotion. Note that k_{HDN2}, k_{HDN3}, and k_{HDN4} are certainly enhanced by the promotion, but the DDN pathway (k_{HDN1}) is negatively affected. Indeed, there is a linear correlation between the k_{HDN1} values and the fraction of nonpromoted MoS_2 edge, as shown in Figure 9 (the fraction of nonpromoted MoS_2 edge was calculated from the deconvoluted IR-CO adsorption spectra, as shown in Table S5 of the Supporting Information). Therefore, the active sites for the DDN route exist on nonpromoted edges, in agreement with refs 41 and 95. This negative effect of promoter addition has been rationalized as a difference between the electronic properties of arrangements of adjacent Mo CUS and arrangements of vacancies containing promoter atoms.[96] In view of the fact that Ni increases the concentration of CUS,[56,97,98] we propose that on MoS_2 catalysts, the presence of isolated CUS promotes the σ-donation from N needed for DDN. In the presence of Ni, however, the concentration of adjacent CUS (including Ni-associated vacancies) increases at the expense of the isolated ones. In such arrangements, the hydrogenation of the aromatic ring is much more favored than DDN.

On the other hand, k_{HDN2} and k_{HDN3} correlate neither with the dispersion of the active phase (estimated either from TEM or NO adsorption) nor with any specific band intensity of the CO-IR spectra. This suggests that the effect of Ni is an indirect one, most likely enhancing the H_2 activation or the surface reaction of adsorbed intermediates. In turn, hydrogenation of OPA and C−N bond cleavage in PCHA may depend on the interplay among the dispersion, the decoration level, and

dx.doi.org/10.1021/cs500034d | ACS Catal. 2014, 4, 1487−1499

support effect of the MoS_2 phase (see below). The variation of k_{HDN4}, in contrast, satisfactorily correlates with the dispersion of the sulfide phase determined by TEM and NO adsorption and the fraction of promoted edge. It has been proposed that the adsorption step leading to hydrogenation occurs via π-donation of the double bond to a single CUS.[69] Therefore, the saturation of the double bond in PCHE is likely to occur on Ni-promoted sites because the Ni−Mo−S phase determines the activity.

Effect of the Support. The primary role of a catalytic support is to maximize and stabilize the concentration of active surface. However, in very few cases the effect of the support is limited to that. In the particular case of supported sulfide catalysts, the carrier may modify the electronic properties, the acid properties, and the morphology of the active phase as well as the promotion effect of Ni or Co.[99−102] According to the described primary role of the support, the activity of the MoS_2 catalysts correlates with the dispersion of the sulfide phase determined from TEM. The surprising decrease of the sulfide dispersion and activity of the catalysts on modified SBA-15, in stark contradiction with previous reports,[20,23,59,60,94] is attributed in the present case to pore blocking during the modification procedures that led to agglomeration of Mo species (note the large differences between the textural properties of catalysts supported on SBA-15 and those supported on Ti- and Zr-modified materials).

The promotion with Ni led to more active catalysts on Ti-SBA and Zr-SBA than on pure SBA-15. This showed that the promotion effect is much more pronounced on the modified supports. In this respect, the changes in activity and the deconvolution of the IR spectra of adsorbed CO (Table S5 of the Supporting Information) indicate that the fraction of promoted MoS_2 edge increases in the support order SBA-15 < Zr-SBA < Ti-SBA < Al_2O_3. Comparison among Ni-MoS_2 catalysts supported on bulk oxides also showed better promotion on Al_2O_3 than on SiO_2, TiO_2, and ZrO_2.[103] Thus, although the exact nature of Ni incorporation into the edges of MoS_2 is unclear, it appears obvious that the nature of the support strongly influences this chemistry. The trend of the promoted MoS_2 edge resembles the trend of the Lewis acid concentration and strength of the supports as inferred from the blue shift of the IR bands attributed to CO adsorbed on Lewis acid sites, that is, SBA-15 (no Lewis sites detected) < Ti-SBA (2184 cm^{-1}) ≤ Zr-SBA (2189 cm^{-1}) < Al_2O_3 (2192 cm^{-1}). Probably the presence of Lewis acid sites favors close interaction between Ni and Mo species, which in turn leads to a high promotion degree.

The catalyst supported on Al_2O_3 is the most active for HDS, which is attributed to the significant Ni incorporation to the MoS_2 edges and the remarkable increase in dispersion. The significant increase in the HDS activity on Ti-SBA after Ni promotion is also attributed to a high decoration level. Furthermore, the rate of OPA hydrogenation on Ti-SBA is the highest, yielding the most active Ni-MoS_2 catalyst for HDN. In a recent work, a Ni-MoS_2 catalyst supported on TiO_2−SBA-15 also exhibited higher HDN rates compared with Ni-MoS_2/ZrO_2−SBA-15.[19] The cause of this high activity is attributed to a support influence on the acidity of Mo and Ni cations. Note that in the deconvoluted IR spectra (Figure S5 of the Supporting Information), the positions of the bands of CO adsorbed on nonpromoted Mo atoms and Ni shift to higher wavenumbers in the sequence SBA-15 (2093 cm^{-1}) < Ti-SBA (2096 cm^{-1}) < Zr-SBA (2100 cm^{-1}) < Al_2O_3 (2112 cm^{-1}) and Ti-SBA (2123 cm^{-1}) < SBA-15 (2124 cm^{-1}) < Zr-SBA (2125 cm^{-1}) < Al_2O_3 (2128 cm^{-1}), respectively. Although the differences in band positions among the SBA-type materials are subtle, the acid strength of the CUS on Al_2O_3 is higher than on the mesoporous materials, as judged from the much larger shifts on Al_2O_3. Hence, we conclude that the lower acid strength of the sulfide phase on Ti-SBA (relative to that on Al_2O_3) yields optimal OPA-active phase interaction, which enhances its hydrogenation.

If we interpret increasing acidity of the sulfide phase of supported Ni-MoS_2 (i.e., stronger electronic transfer toward the support[91]) as increasingly strong support−sulfide phase interactions, then the interaction is the strongest in the case of the catalysts supported on alumina (exhibiting the bands at the highest wavenumbers). Moderate interactions would lead to weaker acidity of adsorption sites on SBA-15-type materials, as suggested by the position of the deconvoluted peaks in the IR spectra. Similarly, moderate support-MoS_2 interactions have been related to high intrinsic activity of MoS_2 catalysts.[103]

In contrast to the Ni-promoted sulfides, the spectra of CO adsorbed on MoS_2 catalysts show the main band of CO adsorbed on the sulfide to appear at lower wavenumbers on Al_2O_3 (2114 cm^{-1}) than on mesoporous materials (>2120 cm^{-1}) (see Figure 3; see also refs 83, 104). We speculate that the strong interaction between Al_2O_3 and Mo species leads to not fully sulfided MoS_2, suggesting that the Al−O−Mo bonds are relatively abundant.[60,105] In turn, the basic character of these bridging oxygen groups may compensate the support-induced acidity of the MoS_2 phase. Alternatively, in ref 105, it is proposed that there is a contribution of weakly interacting CO to the spectra of CO adsorbed on MoS_2/SiO_2, which shifts the observed position to high wavenumbers. The verification of both proposals is, however, out of the scope of this study.

CONCLUSIONS

Purely siliceous SBA-15 as well as Ti- and Zr-modified SBA-15, and Al_2O_3 were used as supports for a series of MoS_2 and Ni-promoted MoS_2 catalysts for the simultaneous hydrodesulfurization (HDS) of dibenzothiophene (DBT) and hydrodenitrogenation (HDN) of *o*-propylaniline. The OPA conversion rates were higher than those of DBT in all cases except for Ni-MoS_2/Al_2O_3, which exemplified the very high HDS activity. OPA reacted preferentially through hydrogenation, and DBT, through direct sulfur removal. The direct denitrogenation of OPA is faster on unpromoted MoS_2 than on Ni-promoted MoS_2. In contrast, the direct desulfurization is much faster on Ni-promoted catalysts compared with nonpromoted ones.

The activity for HDS and HDN of the MoS_2 catalysts was primarily determined by the dispersion of the supported sulfide phase. The hydrodenitrogenation of OPA inhibited the desulfurization of DBT on unpromoted catalysts due to the selective poisoning of coordinatively unsaturated sites. The addition of Ni increased dispersion, concentration of adsorption sites, and intrinsic activity of the sulfide phase in all cases. The effects of Ni addition were attributed to the formation of the Ni−Mo−S phase (corroborated by CO−IR spectroscopy). The composition and, hence, acidity of the support influenced the degree of Ni substitution and acidity of the supported sulfide phase, leading to different impact on the final catalyst.

The HDS rates directly depend on the decoration degree of Ni on the edges of MoS_2 because HDS occurs on sites involving accessible Mo and Ni cations. In contrast, direct hydrodenitrogenation was reduced because only Mo cations are

dx.doi.org/10.1021/cs500034d | ACS Catal. 2014, 4, 1487−1499

catalytically active, whereas the presence of Ni enhances the hydrogenation of the aromatic ring and leads to higher HDN rates via this way. The hydrogenation pathways of OPA and DBT occur on the same active sites, which are tentatively attributed to be brim sites or adjacent CUS.

■ ASSOCIATED CONTENT

Supporting Information

Textural properties of the supports, detailed TEM characterization of sulfide materials (i.e., histograms of length and stacking degree, average, and standard deviation values), complete deconvolution of IR spectra (with integrated areas of all deconvoluted bands), experimental concentration profiles of reactant and products during the kinetic tests compared with those calculated from kinetic modeling, and TOF values for different routes. This material is available free of charge via the Internet at http://pubs.acs.org/.

■ AUTHOR INFORMATION

Corresponding Authors

*Phone: 0049 89 28912827. Fax: 0049 89 28913544. E-mail: Oliver.Gutierrez@mytum.de.

*Phone: 0049 89 28913540. Fax: 0049 89 28913544. E-mail: Johannes.Lercher@ch.tum.de

Notes

The authors declare no competing financial interest.

■ ACKNOWLEDGMENTS

The authors would like to thank Prof. Roel Prins for fruitful discussions and the critical reading of the manuscript and Chevron Energy Technology Company for providing the alumina support.

■ REFERENCES

(1) EU Fuel Regulations, <http://www.dieselnet.com/standards/eu/fuel.php>.
(2) Pawelec, B.; Navarro, R. M.; Campos-Martin, J. M.; Fierro, J.-L. G. *Catal. Sci. Technol.* **2011**, *1*, 23−42.
(3) Stanislaus, A.; Marafi, A.; Rana, M. S. *Catal. Today* **2010**, *153*, 1−68.
(4) Okamoto, Y.; Breysse, M.; Dhar, G. M.; Song, C. *Catal. Today* **2003**, *86*, 1−4.
(5) Breysse, M.; Portefaix, J. L.; Vrinat, M. *Catal. Today* **1991**, *10*, 489−505.
(6) Klimova, T.; Calderon, M.; Ramirez, J. *Appl. Catal., A* **2003**, *240*, 29−40.
(7) Okamoto, Y.; Ochiai, K.; Kawano, M.; Kobayashi, K.; Kubota, T. *Appl. Catal., A* **2002**, *226*, 115−127.
(8) Turaga, U. T.; Song, C. *Catal. Today* **2003**, *86*, 129−140.
(9) Wang, A.; Wang, Y.; Kabe, T.; Chen, Y.; Ishihara, A.; Qiany, W. *J. Catal.* **2001**, *199*, 19−29.
(10) Sampieri, A.; Pronier, S.; Blanchard, J.; Brunet, S.; Fajerwerg, K.; Louis, C.; Pérot, G. *Catal. Today* **2005**, *107/108*, 537−544.
(11) Dhar, G. M.; Kumaran, G. M.; Kumar, M.; Rawat, K. S.; Sharma, L. D.; Raju, B. D.; Rao, K. S. R. *Catal. Today* **2005**, *99*, 309−314.
(12) Vradman, L.; Landau, M. V.; Herskowitz, M.; Ezersky, V.; Talianker, M.; Nikitenko, S.; Koltypin, Y.; Gedanken, A. *J. Catal.* **2003**, *213*, 163−175.
(13) Gutiérrez, O. Y.; Fuentes, G. A.; Salcedo, C.; Klimova, T. *Catal. Today* **2006**, *116*, 485−497.
(14) Huang, Z. D.; Bensch, W.; Lotnyk, A.; Kienle, L.; Fuentes, S.; Bocarando, J.; Alonso, G.; Ornelas, C. *J. Mol. Catal. A* **2010**, *323*, 45−51.
(15) Huang, Z. D.; Bensch, W.; Kienle, L.; Fuentes, S.; Alonso, G.; Ornelas, C. *Catal. Lett.* **2009**, *127*, 132−142.
(16) Sundaramurthy, V.; Eswaramoorthi, I.; Dalai, A. K.; Adjaye, J. *Microporous Mesoporous Mater.* **2008**, *111*, 560−568.
(17) Biswas, P.; Narayanasarma, P.; Kotikalapudi, C. M.; Dalai, A. K.; Adjaye, J. *Ind. Eng. Chem. Res.* **2011**, *50*, 7882−7895.
(18) Mouli, K. C.; Mohanty, S.; Hu, Y.; Dalai, A.; Adjaye, J. *Catal. Today* **2012**, *207*, 133−144.
(19) Soni, K. K.; Mouli, K. C.; Dalai, A. K.; Adjaye, J. *Microporous Mesoporous Mater.* **2012**, *152*, 224−234.
(20) Mendoza, J. A.; Puente, I.; Salcedo, C.; Klimova, T. *Fuel* **2012**, *100*, 100−109.
(21) Ramírez, J.; Gutiérrez, A.; Sánchez, F.; Macías, V.; Castillo, P.; Oliviero, L.; Maugé, F. *Energy Fuels* **2012**, *26*, 773−782.
(22) Kumaran, G. M.; Garg, S.; Soni, K.; Kumar, M.; Sharma, L. D.; Dhar, G. M.; Rao, K. S. R *Appl. Catal., A* **2006**, *305*, 123−129.
(23) Gutiérrez, O. Y.; Valencia, D.; Klimova, T. *J. Catal.* **2007**, *249*, 140−153.
(24) Deepa, G.; Sankaranarayanan, T. M.; Shanthia, K.; Viswanathan, B. *Catal. Today* **2012**, *198*, 152−262.
(25) Suresh, C.; Santhanaraj, D.; Gurulakshmi, M.; Deepa, G.; Selvaraj, M.; Sasi Rekha, N. R.; Shanthi, K. *ACS Catal.* **2012**, *2*, 127−134.
(26) Meier, R. *Vibr. Spectrosc.* **2005**, *39*, 266−269.
(27) Dodd, J. G.; DeNoyer, L. K. In *Handbook of Vibrational Spectroscopy*; Chalmers, J. M., Griffiths, P. R., Eds.; John Wiley & Sons Ltd.: Chichester, 2002; Vol. *3*.
(28) Popov, A.; Kondratieva, E.; Mariey, L.; Goupil, J. M.; El Fallah, J.; Gilson, J. P.; Travert, A.; Maugé, F. *J. Catal.* **2013**, *297*, 176−186.
(29) Afanasiev, P. *J. Catal.* **2010**, *269*, 269−280.
(30) Hensen, E.; Kooyman, P.; van der Meer, Y.; van der Kraan, A.; de Beer, V.; van Veen, J.; van Santen, R. *J. Catal.* **2001**, *199*, 224−235.
(31) Kasztelan, S.; Toulhoat, H.; Grimblot, J.; Bonnelle, J. *Appl. Catal.* **1984**, *13*, 127−159.
(32) Travert, A.; Dujardin, C.; Maugé, F.; Cristol, S.; Paul, J. F.; Payen, E.; Bougeard, D. *Catal. Today* **2001**, *70*, 255−269.
(33) Travert, A.; Dujardin, C.; Maugé, F.; Veilly, E.; Paul, J. F.; Payen, E. *J. Phys. Chem. B* **2006**, *110*, 1261−1270.
(34) Kung, M. C.; Kung, H. H. *Catal. Rev. Sci. Eng.* **1985**, *27*, 425−460.
(35) Travert, A.; Dujardin, C.; Maugé, F.; Veilly, E.; Cristol, S.; Paul, J.-F.; Payen, E. *J. Phys. Chem. B* **2006**, *110*, 1261−1270.
(36) Egorova, M.; Prins, R. *J. Catal.* **2004**, *255*, 417−427.
(37) Wang, H.; Prins, R. *J. Catal.* **2008**, *258*, 153−164.
(38) Pophal, C.; Kameda, F.; Hoshino, K.; Yoshinaka, S.; Segawa, K. *Catal. Today* **1997**, *39*, 21−32.
(39) Bataille, F.; Lemberton, J.; Michaud, P.; Pérot, G.; Vrinat, M.; Lemaire, M.; Schulz, E.; Breysse, M.; Kasztelan, S. *J. Catal.* **2000**, *191*, 409−422.
(40) Houalla, M.; Nag, N.; Sapre, A.; Broderick, D.; Gates, B. *AIChE J.* **1978**, *24*, 1015−1021.
(41) Hrabar, A.; Hein, J.; Gutiérrez, O. Y.; Lercher, J. A. *J. Catal.* **2011**, *281*, 325−338.
(42) Jian, M.; Prins, R. *Catal. Today* **1996**, *30*, 127−134.
(43) Pérot, G. *Catal. Today* **1991**, *10*, 447−472.
(44) Wang, H.; Prins, R. *J. Catal.* **2008**, *258*, 153−164.
(45) Sun, Y.; Prins, R. *J. Catal.* **2009**, *267*, 193−201.
(46) Farag, H.; Sakanishi, K.; Sakae, T.; Kishida, M. *Appl. Catal., A* **2006**, *314*, 114−122.
(47) Gutiérrez, O. Y.; Ayala, E.; Puente, I.; Klimova, T. *Chem. Eng. Commun.* **2009**, *196*, 1163−1177.
(48) Beltramone, A. R.; Crossley, S.; Resasco, D. E.; Alvarez, W. E.; Choudhary, T. V. *Catal. Lett.* **2008**, *123*, 181−185.
(49) Korre, S. C.; Klein, M. T.; Quann, R. J. *Ind. Eng. Chem. Res.* **1997**, *36*, 2041−2050.
(50) Laredo, G. C.; Montesinos, A.; De los Reyes, J. A. *Appl. Catal., A* **2004**, *265*, 171−183.
(51) Egorova, M.; Prins, R. *J. Catal.* **2004**, *221*, 11−19.
(52) Gutiérrez, O. Y.; Hrabar, A.; Hein, J.; Yu, Y.; Han, J.; Lercher, J. A. *J. Catal.* **2012**, *295*, 155−168.

(53) Zhang, X. L.; Ozkan, U. S. *Stud. Surf. Sci. Catal.* **1997**, *106*, 69−82.
(54) Satterfield, C. N.; Yang, S. H. *Ind. Eng. Chem. Process Des. Dev.* **1984**, *23*, 11−19.
(55) Jian, M.; Prins, R. *Ind. Eng. Chem. Res.* **1998**, *37*, 834−840.
(56) Kim, S. C.; Simons, J.; Massoth, F. E. *J. Catal.* **2002**, *212*, 201−206.
(57) Froment, G. F. *Catal. Today* **2004**, *98*, 43−54.
(58) Daudin, A.; Lamic, A. F.; Perót, G.; Brunet, S.; Raybaud, P.; Bouchy, C. *Catal. Today* **2008**, *130*, 221−230.
(59) Klimova, T.; Gutiérrez, O.; Lizama, L.; Amezcua, J. *Microporous Mesoporous Mater.* **2010**, *133*, 91−99.
(60) Gutiérrez, O. Y.; Klimova, T. *J. Catal.* **2011**, *281*, 50−62.
(61) Sun, M.; Adjaye, J.; Nelson, A. E. *Appl. Catal., A* **2004**, *263*, 131−143.
(62) Moreau, C.; Joffre, J.; Saenz, C.; Geneste, P. *J. Catal.* **1990**, *122*, 448−451.
(63) van Gestel, J.; Dujardin, C.; Maugé, F.; Duchet, J. C. *J. Catal.* **2001**, *202*, 78−88.
(64) Yang, S. H.; Satterfield, C. N. *Ind. Eng. Chem. Process Des. Dev.* **1984**, *23*, 20−25.
(65) Daage, M.; Chianelli, R. R. *J. Catal.* **1994**, *149*, 414−427.
(66) Hensen, E. J. M; Kooyman, P. J.; van der Meer, Y.; van der Kraan, A. M.; de Beer, V. H. J; van Veen, J. A. R; van Santen, R. A. *J. Catal.* **2001**, *199*, 224−235.
(67) Da Silva, P.; Marchal, N.; Kasztelan, S. *Stud. Surf. Sci. Catal.* **1997**, *106*, 353−360.
(68) Whitehurst, D.; Isoda, T.; Mochida, I. *Adv. Catal.* **1998**, *42*, 345−471.
(69) Qu, L.; Prins, R. *Appl. Catal., A* **2003**, *250*, 105−115.
(70) Topsøe, H. *Appl. Catal., A* **2007**, *322*, 3−8.
(71) Kibsgaard, J.; Tuxen, A.; Knudsen, K. G.; Brorson, M.; Topsøe, H.; Laegsgaard, E.; Lauritsen, J. V.; Besenbacher, F. *J. Catal.* **2010**, *272*, 195−203.
(72) Temel, B.; Tuxen, A. K.; Kibsgaard, J.; Topsøe, N.; Hinnemann, B.; Knudsen, K. G.; Topsøe, H.; Lauritsen, J. V.; Besenbacher, F. *J. Catal.* **2010**, *271*, 280−289.
(73) Ho, T. C. *Catal. Rev. Sci. Eng.* **1988**, *30*, 117−160.
(74) Ozkan, U. S.; Ni, S.; Zhang, L.; Moctezuma, E. *Energy Fuels* **1994**, *8*, 249−257.
(75) Yang, H.; Chen, J.; Briker, Y.; Szynkarczuk, R.; Ring, Z. *Catal. Today* **2005**, *109*, 16−23.
(76) Ho, T. C. *Ind. Eng. Chem. Res.* **1993**, *32*, 1568−1572.
(77) Rana, M. S.; Navarro, R.; Leglise, J. *Catal. Today* **2004**, *98*, 67−74.
(78) Ozkan, U. S.; Zhang, L.; Ni, S.; Moctezuma, E. *J. Catal.* **1994**, *148*, 181−193.
(79) Song, C.; Ma, X. *Appl. Catal., B* **2003**, *41*, 207−238.
(80) Cristol, S.; Paul, J.; Payen, E.; Bougeard, D.; Hutschka, F.; Clémendot, S. *J. Catal.* **2004**, *224*, 138−147.
(81) Tuxen, A. K.; Füchtbauer, H. G.; Temel, B.; Hinnemann, B.; Topsøe, H.; Knudsen, K. G.; Besenbacher, F.; Lauritsen, J. V. *J. Catal.* **2012**, *295*, 146−154.
(82) Gutiérrez, O. Y.; Zhong, L.; Zhu, Y.; Lercher, J. A. *ChemCatChem.* **2013**, *5*, 3249−3259.
(83) Dujardin, C.; Lélias, M. A.; van Gestel, J.; Travert, A.; Duchet, J. C.; Maugé, F. *Appl. Catal., A* **2007**, *322*, 46−57.
(84) Bodrero, T. A.; Bartholomew, C. H. *J. Catal.* **1983**, *84*, 145−155.
(85) Okamoto, Y.; Kubota, T. *Catal. Today* **2003**, *86*, 31−43.
(86) Gutiérrez, O. Y.; Kaufmann, C.; Lercher, J. A. *ACS Catal.* **2011**, *1*, 1595−1603.
(87) Miciukiewicz, J.; Zmierczak, W.; Massoth, F. E. *Bull. Soc. Chim. Belg.* **1987**, *96*, 11−12.
(88) Zmierczak, W.; Murali-Dhar, G.; Massoth, F. E. *J. Catal.* **1982**, *77*, 432−438.
(89) Valyon, J.; Hall, W. K. *J. Catal.* **1983**, *84*, 216−228.
(90) Topsøe, N. Y.; Tuxen, A.; Hinnemann, B.; Lauritsen, J. V.; Knudsen, K. G.; Besenbacher, F.; Topsøe, H. *J. Catal.* **2011**, *279*, 337−351.
(91) Chen, W.; Maugé, F.; van Gestel, J.; Nie, H.; Li, D.; Long, X. *J. Catal.* **2013**, *304*, 47−62.
(92) Torres, B.; Berhault, G.; Chianelli, R. R. Metal Sulfides. *Encyclopedia of Catalysis*; Wiley: New York, 2002.
(93) Topsøe, H.; Clausen, B.; Massoth, F. *Hydrotreating Catalysis Science and Technology*; Springer-Verlag: New York, 1996.
(94) Klimova, T.; Pena, L.; Lizama, L.; Salcedo, C.; Gutiérrez, O. Y. *Ind. Eng. Chem. Res.* **2009**, *48*, 1126−1133.
(95) Shanthi, K.; Pillai, C. N.; Kuriacose, J. C. *Appl. Catal.* **1989**, *46*, 241−249.
(96) van Gestel, J.; Dujardin, C.; Maugé, F.; Duchet, J. C. *J. Catal.* **2001**, *202*, 78−88.
(97) Besenbacher, F.; Brorson, M.; Clausen, B. S.; Helveg, S.; Hinnemann, B.; Kibsgaard, J.; Lauritsen, J. V.; Moses, P. G.; Nørskov, J. K.; Topsøe, H. *Catal. Today* **2008**, *130*, 86.
(98) Byskov, L. S.; Nørskov, J. K.; Clausen, B. S.; Topsøe, H. Sulphur Bonding in Transition Metal Sulphides and MoS_2 Based Structures. In *Transition Metal Sulphides − Chemistry and Catalysis*; Weber, T., Prins, R., van Santen, R. A., Eds.; Kluwer Academic Publishers: Dordrecht, The Netherlands, 1998.
(99) Breysse, M.; Afanasiev, P.; Geantet, C.; Vrinat, M. *Catal. Today* **2003**, *86*, 5−16.
(100) Hédoire, C. E.; Louis, C.; Davidson, A.; Breysse, M.; Maugé, F.; Vrinat, M. *J. Catal.* **2003**, *220*, 433−441.
(101) Ninh, T. K. T.; Massin, L.; Laurenti, D.; Vrinat, M. *Appl. Catal., A* **2011**, *407*, 29−39.
(102) Hein, J.; Hrabar, A.; Jentys, A.; Gutiérrez, O. Y.; Lercher, J. A. *ChemCatChem.* **2014**, *7*, 485−499.
(103) Laurenti, D.; Phung-Ngoc, B.; Roukoss, C.; Devers, E.; Marchand, K.; Massin, L.; Lemaitre, L.; Legens, C.; Quoineaud, A.-A.; Vrinat, M. *J. Catal.* **2013**, *297*, 165−175.
(104) Cesano, F.; Bertarione, S.; Piovano, A.; Agostini, G.; Mastabur, M.; Groppo, E.; Bonino, F.; Scarano, D.; Lamberti, C.; Bordiga, S.; Montanari, L.; Bonoldi, L.; Millinib, R.; Zecchina, A. *Catal. Sci. Technol.* **2011**, *1*, 123−136.
(105) Hensen, E. J. M.; de Beer, V. H. J.; van Veen, J. A. R.; van Santen, R. A. *Catal. Lett.* **2002**, *84*, 59−67.